Reduced Skeletal Muscle Phosphocreatine Concentration in Type 2 Diabetic Patients: A Quantitative Image-Based Phosphorus-31 MR Spectroscopy Study

Erika M Ripley, PhD[1], Geoffrey D Clarke, PhD[1,2,3], Vala Hamidi, MD[2], Robert A Martinez, MD[2], Floyd D Settles, DMP[1], Carolina Solis, MD[2], Shengwen Deng[3], Muhammad Abdul-Ghani, MD, PhD[2], Devjit Tripathy, MD[2], Ralph A DeFronzo, MD[2]

[1] Department of Radiology, [2]Diabetes Division and [3]Research Imaging Institute, University of Texas Health Science Center at San Antonio, San Antonio, TX

Running Head: Reduced Skeletal Muscle Phosphocreatine Concentration in T2DM

Word Count:
Abstract = 249
Manuscript = 5083
# Figures = 8
#Tables = 2

Please address correspondence to:

Ralph A DeFronzo, MD
Texas Diabetes Institute and Diabetes Division
University of Texas Health Science Center at San Antonio
7703 Floyd Curl Drive
San Antonio TX 78229-3900
albarado@uthscsa.edu

Revised 02/27/2018

ABSTRACT

Mitochondrial function has been examined in insulin resistant (IR) states including type 2 diabetes mellitus (T2DM). Previous studies using phosphorus-31 magnetic resonance spectroscopy (^{31}P-MRS) in T2DM reported results as relative concentrations of metabolite ratios, which could obscure differences in phosphocreatine [PCr] and adenosine triphosphate [ATP] between T2DM and NGT individuals. We used image-guided ^{31}P-MRS method to quantitate [PCr], inorganic phosphate [Pi], phosphodiester [PDE] and [ATP] in vastus lateralis (VL) muscle in 11 T2DM and 14 NGT subjects. Subjects also received OGTT, euglycemic insulin clamp, ^{1}H-MRS to measure intramyocellular lipids [IMCL] and VL muscle biopsy to evaluate mitochondrial density. T2DM subjects had lower absolute [PCr] and [ATP] than NGT subjects (PCr: 28.6 ± 3.2 vs 24.6 ± 2.4, $p< 0.002$) and (ATP: 7.18 ± 0.6 vs 6.37 ± 1.1, $p< 0.02$) while [PDE] was higher, but not significantly. [PCr], obtained using the traditional ratio method, showed no significant difference between groups. [PCr] was negatively correlated with HbA1c ($r=-0.63$, $p<0.01$) and fasting plasma glucose ($r=-0.51$, $p=0.01$). [PDE] was negatively correlated with Matsuda Index ($r=-0.43$, $p=0.03$) and M/I ($r=-0.46$, $p=0.04$), but was positively correlated with [IMCL] ($r=0.64$, $p<0.005$), HbA1c and FPG ($r=0.60$, $p=0.001$). To summarize, using a modified, *in vivo* quantitative ^{31}P-MRS method, skeletal muscle [PCr] and [ATP] are reduced in T2DM, while this difference was not observed with the traditional ratio method. The strong inverse correlation between [PCr] versus HbA1c, FPG, and insulin sensitivity supports the concept that lower baseline skeletal muscle [PCr] is related to key determinants of glucose homeostasis.

Revised 02/27/2018

Keywords. Phosphorus-31 magnetic resonance spectroscopy, skeletal muscle metabolism, type 2 diabetes, insulin resistance, mitochondrial function, phosphocreatine, ATP

Glossary. ADP, adenosine diphosphate; ATP, adenosine triphosphate; BMI, body mass index; BW, receiver bandwidth; FPG, fasting plasma glucose; G-3-P, glycerol-3-phosphate; GDE5, a mammalian muscle phosphodiesterase; GPC, glycerophosphocholine; GPC-PDE, glycerophosphocholine phosphodiesterase; HbA1c, glycated hemoglobin; HDL, high-density lipoprotein; H^+, hydrogen ion; ^{1}H-MRS, hydrogen-1 magnetic resonance spectroscopy; IMCL, intramyocellular lipid; K_{eq}, equilibrium constant; MDP, methylenediphosphonic acid; mRNA, messenger ribonucleic acid; pH, potential of hydrogen; Pi, inorganic phosphate; NGT, normal glucose tolerance; NSA, number of signals averaged; OGTT, oral glucose tolerance test; PCr, phosphocreatine, PDE, phosphodiester, ^{31}P-MRS, phosphorus-31 magnetic resonance spectroscopy; δ, chemical shift; SSPI, steady-state plasma insulin concentration; T1, longitudinal relaxation time; T2, transverse relaxation time; T2DM, type 2 diabetes mellitus; tCr, total creatine; TE, echo time; TEM, transmission electron microscopy; TGD, total glucose disposal; TR, pulse repetition time; VL, vastus lateralis; IMCL, intramyocellular lipid.

Revised 02/27/2018

INTRODUCTION

Skeletal muscle mitochondrial function and impaired ATP production have been described in insulin resistant (IR) states, including type 2 diabetes mellitus (T2DM) (3, 46). However, there is controversy as to whether the mitochondrial function is the cause of or result of insulin resistance. Phosphorus-31 magnetic resonance spectroscopy (^{31}P-MRS) has been used to study mitochondrial function by measuring phosphorus metabolites under a range of physiological conditions and relating intramyocellular levels to the presence of skeletal muscle insulin resistance (55). Using MR spectroscopic techniques *in vivo*, impaired skeletal muscle mitochondrial function has been demonstrated in a variety of insulin resistant states including the elderly (41), insulin-resistant offspring of T2DM individuals (9, 35, 42), T2DM subjects (2, 43, 52, 53, 55), and obese subjects (38, 46, 61).

Traditionally, results from *in vivo* ^{31}P-MRS in T2DM individuals have been expressed as ratios of phosphorus metabolites, under the assumption that the ATP concentration ([ATP]) in resting muscle is uniform and constant across all subjects. Data to support the constancy of muscle ATP levels is lacking and reliance on this assumption could obscure simultaneous changes in phosphorus metabolites, attenuating or enhancing metabolic differences between T2DM and NGT. Therefore, development of a ^{31}P MRS method to provide absolute concentrations of intramyocellular phosphorous metabolites is essential to precisely assess the contribution of mitochondrial function to metabolic processes (28).

The aims of this study were (i) to develop a reproducible method to quantitate phosphorus metabolites in human vastus lateralis (VL) muscle using MRS, (ii) to

Revised 02/27/2018

compare differences between NGT and T2DM subjects in basal [ATP], inorganic phosphate [Pi], phosphocreatine [PCr], phosphodiester [PDE] and creatine [Cr], and (iii) to examine the relationship between phosphorous metabolite concentrations and measures of glycemic control, insulin resistance, mitochondrial density and intramyocellular lipid content.

MATERIALS AND METHODS

Subjects

Fourteen NGT and 11 T2DM subjects, matched for age, gender and BMI, participated in the study (Table 1). All subjects had normal liver, cardiopulmonary, and kidney function as determined by medical history, physical examination, screening blood tests, electrocardiogram, and urinalysis. No subject was taking any medication known to affect glucose tolerance. Body weight was stable (± 1.4 kg) for at least 3 months before the study in all subjects and no subject participated in an excessively heavy exercise regimen or took part in any exercise program over the 48 hours prior to study. NGT subjects had no family history of T2DM. T2DM subjects were on a stable dose (at least 3 months) of monotherapy with metformin or metformin combined with sulfonylurea. All patients were diagnosed with T2DM for at least a year.

Studies were performed at 0800 hours following a 10-hour overnight fast. Subjects received a 2-hour 75 g oral glucose tolerance test (OGTT). Hydrogen -1 and ^{31}P MRS were performed on the VL muscle at the Research Imaging Institute within one week of the OGTT. On a separate day, a subset of subjects (9 T2DM and 12 NGT) received euglycemic insulin clamp and VL muscle biopsy. The study protocol was approved by Institutional Review Board of University of Texas Health Science Center, San Antonio,

Texas, and informed written consent was obtained from all subjects before participation.

Oral Glucose Tolerance Test

Before the start of OGTT, a catheter was placed into an antecubital vein and blood samples were collected at -30, -15, and 0 minutes. Subjects then ingested 75 g of glucose, and blood samples were obtained at 30, 60, 90, and 120 minutes for determination of plasma glucose, FFA, and insulin concentrations. Insulin sensitivity during the OGTT was assessed by the Matsuda index (MI) (33). The insulin secretion/insulin resistance (disposition) index, an indicator of beta cell function, was calculated as (Δ AUC-I/Δ AUC-G) x MI (1).

Magnetic Resonance Spectroscopy

At 0800 hours after an overnight fast, ^{31}P-MRS measurements of hydrogen- and of phosphorus-containing metabolites were obtained from the right VL muscle using a 3 Tesla MRI system (TIM Trio, Siemens Medical, Malvern PA). Quantitation of intramyocellular lipids [IMCL] was determined using single-voxel ^{1}H-MRS with the internal reference method. Subjects were positioned in a supine, feet first orientation with the right upper leg as close to the center of the magnet as possible. A 4-channel receive-only array flex coil (Siemens) was wrapped around the right thigh and the leg was stabilized. Two stimulated echo acquisition mode (STEAM) MRS sequences were acquired, one with the water peak intact (15 mm x 15 mm x 15 mm, TR = 3 s, TE = 30 ms, NSA = 16) and another at the same location with the water peak suppressed (15 mm x 15 x 15 mm, TR = 3 s, TE = 270 ms, NSA = 128).

For the ^{31}P-MRS measurements, a rigid ^{31}P/^{1}H dual-tuned circular, saddle-shaped (18 cm diameter) surface coil (Rapid Biomedical, Rimpar, Germany) was used. RF coil

testing indicated that the shape of the sensitive volume changed with movements that alter the RF coil orientation relative to the main, B_o field. To ensure study-to-study reproducibility, a holder was devised that fixed the RF coil to the table to maintain the shape and size of the RF coil sensitive constant. Tests of the excitation pulse flip angle with spatial depth and applied RF power demonstrated a broad maximum over the range of 3-5 cm deep from RF coil midline for 50-70 V applied to produce a putative 160^o flip angle. Since the VL muscle is in an anterior compartment of the quadriceps muscle group, the RF coil was positioned as close as possible to isocenter under the right VL muscle with the subjects positioned head first and prone in the magnet. A 6-mL plastic vial with an 850-mM concentration of methylenediphosphonic acid (MDP) was fixed at the center of the coil and used as an external reference. (Figure 1A) MDP was used because its resonance frequency of ~22 ppm downfield from PCr, to avoid overlapping relevant metabolite peaks. In addition, MDP is safe when diluted, is water soluble, and can be placed in a sealed container.

An axial ^{1}H-MRI localizer (35 slices, 200×169×5 mm, TR/TE=498/6.47 ms, BW=120 Hz/px) was acquired for guidance of the spectroscopy slab placement. A ^{1}H-MRS voxel (20×20×10 mm^3, TR/TE=3000/150 ms, NSA=8, BW=1200 Hz), placed in the right VL muscle, was shimmed to a FWHM of water ~20 Hz. The acquired shim values were also used for the ^{31}P-MRS sequences. The axial images were used to position a paracoronal, five-slice ^{1}H-MRI scan (TR/TE = 450/6.15 ms; thickness 5 mm; FOV = 187×250 mm; matrix = 192×256, BW=120 Hz/pixel) which was positioned in the same way as the subsequent ^{31}P-MRS slab, both in the muscle and the phantom, to estimate the volume of muscle tissue contained within the ^{31}P-MRS slice. Using the reference,

axial ^{1}H-MRI images of the upper right leg, a ^{31}P-MRS slab was positioned in the VL muscle to exclude as much subcutaneous fat and bone as possible (Figure 1A). However, if signal from adipose tissue was inadvertently included, it should not affect the results since there is no PCr in adipose tissue and [ATP] is only ~ 50 μmol/g wet weight (20). A slice-selective ^{31}P-MRS sequence (TR/TE = 10,000/2.3 ms, NSA=16, slice thickness 25mm, BW=3000 Hz) was performed in the quadriceps muscle of the subject and in the leg phantom, as described below.

After the subject was scanned, a 15-cm diameter, 4 L plastic cylindrical leg phantom containing 35 mM phosphoric acid (H_3PO_4) was placed on the coil and a five-slice, para-coronal MRI scan was acquired followed by an MRS scan. Both the phantom 5-slice MRI and phantom ^{31}P-MRS slabs were scanned with the same parameters and slab positions, relative to the RF coil, that were used previously so that the data were collected from the same area within the radio frequency excitation field of the coil. Also, the same ^{31}P-MRS sequence was used with the position centered over the vial of MDP, first with the subject and then with the leg phantom. The change in the MDP peak area, which is due to the changes of the coil's RF field, was used to correct for the effect of coil loading on the metabolite peak height (28). The position of the MDP vial did not change relative to the coil throughout the experiment. The experimental set-up and representative ^{31}P-MRS muscle spectra are shown in Figure 1B.

To examine the reproducibility of the method, 5 healthy NGT subjects (2 males/3 females; age = 39±22 years; BMI = 25.1±4.8 kg·m^{-2}) were studied on two separate occasions within an interval of 5-7 days. Reproducibility was expressed using the coefficient of variation (CV) calculated as the standard deviation (SD) between an

individual's two visits divided by the mean of the two visits. The intra-subject CV and the inter-subject CV also were calculated for each parameter. The same sequence using the MRS slab with varying TR values (0.5, 1, 3, 6, 10 s) in these volunteers also was used to validate that TR=10,000 ms was sufficient avoid T1 corrections in the quantitation calculation.

Euglycemic Insulin Clamp and Muscle Biopsy

Approximately one week after the MRS study, subjects returned at 0800 h for a 4-hour euglycemic insulin clamp (17). A prime-continuous insulin infusion (80 mU/kg·min) was started at time 0 via a catheter placed into the antecubital vein and continued throughout study. A second catheter was placed retrogradely into a vein on the dorsum of hand, which was placed in a heated box (60°C). Baseline arterialized venous blood samples for determination of plasma glucose and insulin were drawn at -30, -20, -10, -5, and 0 min. After the start of insulin, plasma glucose concentration was allowed to decrease to 100 mg/dL, at which level it was maintained by variable infusion of 20% glucose solution. During the insulin clamp, blood samples were drawn every 5–15 min for determination of plasma insulin and glucose concentrations. At the high insulin infusion rate employed in the present study, endogenous glucose production is suppressed by > 90% in NGT and T2DM subjects and the mean glucose infusion rate during the last 60 minutes provides a measure of total body glucose disposal (TGD). TGD divided by the steady state plasma insulin (SSPI) concentration during the 180 - 240 min duration also was calculated.

Vastus lateralis muscle biopsy was performed 60 minutes prior to the start of insulin infusion. The VL muscle specimen was immediately fixed in phosphate buffered 4%

formaldehyde, 1% glutaraldehyde (pH 7.4) at 4°C for several hours and post fixed in 1% osmium tetroxide for 1 hour at room temperature, dehydrated in a series of ethanol dilutions, and embedded in epoxy resin (EMBed 812). Electron microscopy was performed on a JEOL 1230 by an operator blinded to the study. The density of mitochondria was estimated using the point-counting method in a blinded fashion. For each subject, the number density measurements from a minimum of seven images were averaged.

Mitochondrial ATP Synthesis

Mitochondrial ATP synthesis rate was measured *ex vivo* with the chemiluminescence technique, as previously described (3). Briefly, mitochondria were isolated from fresh muscle tissue by differential centrifugation, with 4 mg of mitochondrial protein aliquoted to each reaction well. Substrates were added as follows: 2.5 mM pyruvate, 2.5 mM glutamate, 5 mM succinate plus 0.001 mM rotenone, and palmitoyl-L-carnitine. Malate (2.5 mM) was added to complex I substrates. Luciferine/luciferase was added to monitor ATP production. Substrates were added after 5 min of incubation at 37°C, and the reaction was started by addition of ADP.

Analytical Determinations

Plasma glucose was measured by the glucose oxidase method (Beckman Instruments, Fullerton, CA). Plasma insulin was measured by radioimmunoassay (Diagnostic Products Corp., Los Angeles, CA). Plasma FFA was determined by the enzymatic colorimetric quantification method (Wako Chemicals, Neuss, Germany).

MR Spectroscopy Calculations

The processing of [IMCL] data assumed only a slight variation in the water content in

muscle tissue among individuals. The H_2O signal from the unsuppressed ^{1}H-MRS acquisition was corrected for proton density and relaxation effects to calculate the concentration of IMCL. The concentration of water was calculated as:

$$[H_2O] = W_C/\rho_M \times \rho_W / MM_W \quad [1]$$

where W_C is the water content in muscle tissue (76%), ρ_M is the density of muscle tissue (1.06 g/ml wet weight), ρ_W is the density of water (1.0 g/ml) and MM_W is the molecular weight of water (18 g/mol). Then [IMCL] was calculated in mmol/kg ww by,

$$[IMCL] = [H_2O] \times A_{IMCL}/A_{H2O} \times n\ H_2O/n\ IMCL \times k\ H_2O/k\ IMCL, \quad [2]$$

where $[H_2O]$ is from Eq. 1, A_{IMCL} and A_{H2O} are the fitted amplitudes from AMARES, n is the number of protons for IMCL and H_2O (62 protons/molecule and 10 protons/molecule, respectively) and k_{H2O} and k_{IMCL} are the T1 and T2 relaxation corrections for water and IMCL, respectively, with

$$k_{H2O} = e(-TE/T2) \times (1-e(-TR/T1)), \quad [3]$$

where TE and TR are the ^{1}H-MRS STEAM scan parameters, and T1 and T2 relaxation times for water and IMCL are the published values for VL muscle (60).

Decreased *in vivo* mitochondrial oxidative phosphorylation (OxPhos) has been inferred from changes in the apparent flux of ATP, reported from ^{31}P-MRS studies in a variety of IR states, including T2DM. ^{31}P-MRS allows the evaluation of muscle energetics in vivo: (i) by methods using magnetization transfer, (ii) by measuring the concentrations of phosphorus-containing metabolites; and (iii) by measuring the rate of recovery of the PCr signal following exercise which is a metric for the rate of oxidative ATP synthesis assuming that the CK reaction is much faster than oxidative ATP

Revised 02/27/2018

production; and (iv) in conjunction with ^{1}H-MRS measurements of total creatine concentration [tCr], allowing calculations of adenosine diphosphate concentrations, [ADP], which can yield important information regarding the free energy of ATP hydrolysis. [ADP] is calculated in the literature either assuming a constant level of total creatine [tCr] = [PCr] + [Cr] (5) or that 15% of the total creatine is phosphorylated (49). It is not known whether these assumptions are appropriate for all subjects, especially those with metabolic disorders, so the absolute concentration of creatine, [Cr], was determined directly from the ^{1}H-MRS data in this study.

$$[Cr] = [H_2O] \times (A_{Cr}/A_w) \times (n_w/n_{Cr}) \times (k_w/k_{Cr}) \times WC, \qquad [4]$$

where $[H_2O]$ is the concentration of the muscle water, A_{Cr} is the amplitude of the creatine metabolite peak from the water suppressed scan, A_w is the amplitude of the H_2O peak from the water reference spectrum, n_w and n_{Cr} are the number of protons in water and creatine, and k_w and k_{Cr} are the T1 and T2 relaxation corrections for water and Cr, respectively, with $k = e^{(-TE/T2)} \times (1-e^{(-TR/T1)})$. $[H_2O]$ and WC, the water content factor, were assumed to be 55,556 mM/L and 77%, respectively (63).

For the ^{31}P-MR spectra, (Figure 1B), the volume of the subject's muscle in the MRS slab was determined from the para-coronal, five-slice MR image data from the patient. A similar calculation was performed on the five-slice MR image data from the H_3PO_4 phantom. Hand-drawn contours in the inferior-superior extrema on each of the five images were used to determine the muscle area in each slab. Variability in the definition in muscle margins on these images led to an estimated error of 3%-5%. The signal drop-off changes due to differences in RF coil coupling to the subject versus the H_3PO_4

phantom were compensated by performing the same measurement on 35 mM H_3PO_4 phantom and using the signal from the MDP vial to compensate for coil loading.

The AMARES fitting algorithm within jMRUI 5.0 was used to analyze all spectra (37). [PCr] was determined using our modified, quantitative method as well as with the conventional relative determination, previously described (48). [ATP] was determined from the fitted height of the γATP peak. Muscle pH was measured based on the chemical shift difference between Pi and PCr. In a subset of subjects, muscle creatine concentration [Cr] and intramyocellular lipid [IMCL] concentrations were determined using single-voxel ^{1}H-MRS as previously described (11, 62). Thus, the [PCr] (and by analogy, [ATP], [PDE] and [Pi]) was determined by modifying an equation, proposed by Kemp (28) based on the method of Roth et al (47):

$$[PCr] = [H_3PO_4] \times (A/A_p) \times (A_{MDPref}/A_{MDP}) \times (V_p/V) , \qquad [5]$$

where $[H_3PO_4]$ is the concentration of phosphoric acid in the leg phantom, A is the amplitude of the metabolite peak in the subject, A_p is the amplitude of the H_3PO_4 peak from the phantom, A_{MDPref} is the amplitude of the MDP peak with the phantom, A_{MDP} is the amplitude of the MDP peak with the coil on the leg, V_p is the volume of the phantom in the slab and V is the volume of the subject's muscle in the slab. $[PCr]_{conv}$ also was calculated using the conventional assumption that $[ATP]_{conv}$ is 8.2 mM (24, 48). $[PCr]_{conv}$ = 8.2 mM × (A_{PCr}/A_{ATP}), where A_{PCr} is the amplitude of the PCr peak and A_{ATP} is the amplitude of the γATP peak in the subject. Similarly, $[PDE]_{conv}$ was also calculated using the $[ATP]_{conv}$ = 8.2 mM assumption.

Muscle pH was determined from the chemical shift difference between PCr and Pi (δ), in parts per million (ppm), in the ^{31}P-MRS spectrum with the formula:

317 $$pH = 6.75 + \log[(\delta-3.27)/(5.69-\delta)] \quad [6]$$

318 [ADP] was calculated as: $[ADP] = ([ATP][tCr])/([PCr][H^+] K_{eq})$, using the calculated pH
319 ($H^+ = 10^{pH}$), a creatine kinase equilibrium constant (K_{eq}) of 1.66×10^9 /mol (47), and the
320 [ATP], total creatine concentration ([tCr]), and [PCr] values from the quantitated MRS
321 measurements. $[ADP]_{conv}$ also was calculated using the conventional assumptions of
322 $[ATP]_{conv}$ = 8.2 mM and total creatine concentration ([PCr]+[Cr]) is 42.5 mM (24, 28, 48).

323 Statistics

324 Values are expressed as mean ± SD. Between group comparisons were performed
325 using the Student's two-tailed t-test. Correlation analysis was performed using
326 Pearson's product-moment correlation method for the baseline metabolite
327 concentrations with the following parameters: HbA1c, FPG, Matsuda Index (MI), IS/IR
328 index, insulin sensitivity index (M/I) during the clamp and mitochondrial density. All
329 statistical analyses were performed using the R statistical package (58) with
330 significance at $p < 0.05$.

331

332 **RESULTS**

333 Subjects did not differ significantly in age, weight, sex and BMI (Table 1). As expected,
334 T2DM subjects had higher FPG, HbA1C, fasting plasma triglycerides and lower HDL
335 cholesterol (Table 1). The Matsuda Index of insulin sensitivity (OGTT) and TGD and
336 TGD/SSPI during insulin clamp were significantly reduced in T2DM vs NGT (Table 1).
337 The absolute quantitation of [PCr] had a mean coefficient of variation for repeated
338 measurements in the same individual of 5.2 %. Measured muscle volumes for the

T2DM and NGT subjects were 430.2±64.6 cm^3 and 428.4±68.5 cm^3 respectively (p=0.95). The average PCr linewidth was 21.6±8.7 Hz.

Resting VL muscle [PCr] was reduced in T2DM (24.6 ± 2.4 mM) versus NGT (28.6 ± 3.2 mM, p = 0.002) (Table 2) and correlated inversely with FPG (r = -0.51, p = 0.01) and HbA1c (r = -0.63, p < 0.001) (Figure 2A and 2B). VL muscle [ATP] was reduced in T2DM (6.37 ± 1.05 mM) compared to NGT (7.18 ± 0.60 mM, p = 0.02) subjects. Of note, the [ATP] in VL muscle in both NGT and T2DM subjects was lower than the reference concentration of ATP (8.2 mM) used in the literature (24, 48). [PCr] was significantly and positively correlated with [ATP] (Figure 2C) and negatively correlated with [PDE] (Figure 2D). [ADP] did not differ significantly between NGT and T2DM subjects using our quantitative method, while it was significantly higher in T2DM using the conventional method which assumes a constant concentration for ATP (Table 2).

There were no differences in [Pi], pH, and [Cr] between T2DM and NGT subjects. [IMCL] was significantly increased (p=0.004) in T2DM (8.99 ± 1.46 mmol/kg) vs NGT subjects (6.87 ± 1.15 mmol/kg). (Table 2) [IMCL] was significantly and positively correlated with fasting plasma glucose (r=0.53, p=0.03), and hemoglobin A1c (r=0.59, p=0.007) (Figure 3A). [IMCL] was significantly and negatively correlated with the Matsuda Index of insulin sensitivity (r=-0.60, p=0.009) (Figure 3B) and insulin sensitivity (M/I) measured with the insulin clamp (r=-0.54, p=0.03) in subjects with NGT and T2DM. (Figure 3C) [IMCL] also was negatively correlated with [PCr] (r=-0.43, p=0.074) and was significantly and positively correlated with [PDE] (r=0.64, p<0.005) (Figure 3D).

Myocellular [PDE] was significantly higher in the T2DM versus NGT (4.04+0.98 mM vs. 3.11+0.82 mM, p=0.02). $[PDE]_{conv}$ also was significantly greater (p=0.005) in T2DM VL

Revised 02/27/2018

muscles (5.35+1.6 mM) compared to NGT (3.72+1.05 mM). PDE was positively associated with HbA1c (Figure 4A) and to FPG (r = 0.60, p=0.001) across all participants (Figure 4B). [PDE] correlated negatively with Matsuda Index and insulin sensitivity index (Figure 4C and 4D). However, [PDE] was not associated with BMI or mitochondrial density.

Mitochondrial density was measured with transmission electron microscopy (TEM) in 8 NGT and 6 T2DM subjects; no difference was noted between the two groups (p = 0.96). However, mitochondrial density was negatively correlated with [PCr] (r = -0.67, p = 0.009), [Pi] (r = -0.61, p = 0.02), and [ATP] (r = -0.63, p = 0.02) (Figure 5). TEM examination revealed a loss of muscle mitochondrial structural arrangement and increased lipid droplets in T2DM subjects (Figure 6). [IMCL] correlated negatively with [PCr] in the NGT group, while it correlated positively with [PCr] in the T2DM group (Figure 7A and 7B), even though the two groups were well-matched for age (p = 0.92) and BMI (p = 0.82). No difference in ATP synthesis rate was observed between T2DM and NGT subjects in VL muscle *ex vivo* with any substrate (Figure 8).

DISCUSSION

^{31}P-MRS is a noninvasive method commonly used to provide information about concentrations of intramyocellular high energy phosphate compounds and to assess mitochondrial function. Few human studies have attempted to measure absolute concentrations of these metabolites in the post absorptive state and conflicting results have been reported (15, 52, 55). De Feyter et al. (15) measured resting PCr, Pi, and ADP concentrations using a constant value for [ATP]=8.2 mM and reported no difference between NGT, pre-diabetic and long-standing insulin-treated type 2 diabetic

subjects. Schrauwen-Hinderling et al. (53) reported a 45% delay in PCr recovery half-time in T2DM versus NGT individuals but found no difference in resting Pi/PCr between the two groups. Scheuermann-Freestone et al. (50) reported lower baseline metabolite concentrations in cardiac but not skeletal muscle. Wu et al. (64) reported reduced resting skeletal muscle [Pi], [PCr], and [ATP] by assuming that the β-ATP for the control subjects at rest was equivalent to 5.5 mmol/kg of wet muscle weight.

One possibility that could explain the inconsistent data reported in the literature relates to the use of the conventional ratio method instead of absolute [PCr] and [ATP] quantitation. Use of an assumed constant value for [ATP] can obscure simultaneous decreases in both [PCr] and [ATP] and enhance otherwise marginal differences. Furthermore, the assumption of a uniform and constant [ATP] = 8.2 mM has not been validated in human skeletal muscle. This value originates from a study of 81 young healthy human subjects of indeterminate sex with an age range of 18 – 30 years (24). The muscle samples were obtained from the VL muscle using a percutaneous needle biopsy and were frozen within 4.2 ± 0.8 seconds, powdered, and assayed. The investigators showed a highly significant variance between individuals, suggesting that a single value should not be assumed for all individuals. Further, metabolite concentrations were reported in mmol/kg dry mass and assumptions were used to convert the values into mmol/L of intracellular water, finally arriving at a mean ATP concentration of 8.2 mM.

In the current study, we developed a reproducible method to quantitate ^{31}P-MRS measurements in human VL muscle. Using this modified *in vivo* quantitative imaging method, we found significantly lower [PCr] and [ATP] in VL muscle in T2DM compared

Revised 02/27/2018

to NGT subjects. This finding has important physiologic, as well as clinical implications. Although reduced muscle [PCr] and [ATP] should not be construed to be synonymous with impaired mitochondrial function, they are consistent with a defect in mitochondrial function and could be contribute to the insulin resistance in T2DM individuals (2, 3, 9, 14, 26, 34, 46). Controversy exists about whether the defect in mitochondrial function is responsible for the insulin resistance, i.e. primary or secondary to the insulin resistance (2, 3). Incubation of mitochondria with FFA can cause impaired mitochondrial function, while infusion of lipid to elevate the plasma FFA concentration *in vivo* impairs mitochondrial function and induces insulin resistance (2, 3). Conversely, in a GWAS study arylamine N-acetlytransferase 2 has been identified as an insulin sensitivity gene in humans (29) and of deficiency of Nat2 (mouse homolog of Nat1) in mice leads to reduced mitochondrial function, increased muscle lipid deposition, and insulin resistance (13). Thus, it appears that defective mitochondrial function can both be the cause of, or result from, insulin resistance. Lower [PCr] and [ATP] concentrations have been reported from a freeze-clamped human skeletal muscle biopsy study taken from T2DM subjects following 10-week exposure to metformin (36). However, the significance of this observation is unclear since metformin is not an insulin sensitizing drug in muscle (4) and, when ^{11}C-metformin is given intravenously, it cannot be detected in skeletal muscle (25). In mice, metformin has been reported to inhibit respiratory chain complex I, resulting in decreased hepatic ATP levels and activation of AMPK (22). However, the dose of metformin used in these studies was in the supraphysiologic range. Therefore, we do not believe that background metformin can explain the reduced levels of [PCr] and [ATP] in the present study.

In the current study, differences in mitochondrial number or density between the T2DM and NGT groups were not observed. However, there were clear alterations in muscle architecture of T2DM patients, characterized by intermittent loss of pairing along the Z line and altered regularity of the pairing. Mitochondrial density correlated negatively with the resting concentration of phosphorus metabolites [PCr], [Pi], and [ATP], indicating that individuals with a greater quantity of mitochondria had lower baseline cytosolic phosphorus levels. This could be related to the previously described reduction in the number of subsarcolemmal mitochondria in T2DM patients, which are hypothesized to be functionally and structurally distinct from intermyofibrillar mitochondria (45).

Previous light and electron microscopy studies in healthy NGT subjects have demonstrated that mitochondria in skeletal muscle are arranged in a highly ordered manner, with the highest mitochondrial density found the subsarcolemmal region of type I fibers (54). Reduced size, but not lower density of mitochondria, has been reported in human skeletal muscle in T2DM (26), although one study reported reduced mitochondrial densities in offspring of IR individuals (35). Intergenerational manifestations of insulin resistant phenotypes may result from genetic (13, 29, 40) or epigenetic causes (19, 31).

We also found [IMCL] to be significantly higher in T2DM subjects than in age- and BMI-matched NGT subjects, consistent with previous publications from our lab (6, 7) and others (16, 23, 30, 39, 57, 59). [IMCL] correlated strongly with measures of glycemic control and insulin sensitivity including HbA1c, FPG, Matsuda Index, and M/I, insulin sensitivity index (Figure 3). The increased [IMCL] is consistent with previous findings with MRS (7, 16, 21, 23, 30) and with increased intramyocellular levels of fatty acyl

454 CoA, diacylglycerol (DAG) and ceramides with muscle biopsy (3, 6, 26, 32). Further,
455 increased intramyocellular levels of toxic lipid metabolites have been shown to inhibit
456 insulin signaling and to correlate closely with defects in insulin resistance in T2DM and
457 obese NGT individuals (8, 10).

458 In the present study we also observed increased skeletal muscle PDE concentrations
459 by ^{31}P-MRS. Although less well appreciated than increase intramyocellular levels of
460 FACoAs, DAG and ceramides, elevated muscle [PDE] also has been associated with
461 advancing age, lower resting mitochondrial activity, obesity and insulin resistance (56,
462 61). Using high-resolution ^{31}P-MRS (7 Tesla), the main component of the PDE peak in
463 skeletal muscle has been shown to be glycerophosphocholine (GPC). (61) In the
464 present study we also observed an increase in muscle [PDE] in T2DM versus NGT
465 subjects. (Table 2). Further, muscle [PDE] was closely associated with insulin
466 resistance using both the Matsuda index of insulin sensitivity and insulin resistance
467 index (M/I) during the insulin clamp, as well as with indices of glycemia and [IMCL]
468 (Figure 4). These results suggest that increased [PDE] should be added to the list of
469 intramyocellular metabolites that contribute to insulin resistance in T2DM individuals. In
470 T2DM individuals, [IMCL] was increased and correlated positively with [PCr], while in
471 NGT individuals it correlated negatively with [PCr]. Because diabetic skeletal muscle is
472 resistant to insulin-stimulated glucose uptake (18), it is forced to switch to lipid oxidation
473 in order to generate energy in the form of ATP. This could explain the elevated [IMCL]
474 and positive correlation between [IMCL] and [PCr]. In contrast, skeletal muscle in NGT
475 subjects is normally sensitive to insulin-stimulated glucose uptake and relies upon
476 glucose as its primary energy source. This would explain the negative relationship

between [IMCL] and [PCr] and reduced (compared to T2DM subjects) muscle [IMCL]. This study has several limitations. The number of subjects is relatively small, obese non-diabetic subjects were not studied and the age range did not include very young or very old individuals (range = 31-70 years). (5, 21, 37, 44) VO_2max was not measured, although all subjects were considered to be sedentary on the basis of a routine exercise questionnaire and no subject participated in a routine or excessively heavy exercise program. A dedicated study to examine the effect of VO_2max and exercise training on phosphorus metabolite concentrations in VL muscle would be of great interest (5, 21, 38, 44), since the maximum rate of oxygen consumption VO_{2max} is reduced in T2DM individuals (43). Further studies examining the relationship between body fat composition/distribution and muscle phosphorus metabolites also would be of interest. Due to the limited size of the biopsy samples, direct measurements of lipid content/type could not be performed and subsarcolemmal and intermyofibrillar fractions were not examined (45). Future studies using the absolute quantitative method to measure PCr recovery time to assess *in vivo* mitochondrial capacity in combination with measurement of the activity of mitochondrial oxidative enzymes and mRNA expression of phosphodiesterase and regulators of mitochondrial biogenesis in muscle biopsy specimens would provide additional insights.

In summary, using a modified *in vivo* quantitative imaging method, we have demonstrated that skeletal muscle [PCr] and [ATP] are reduced in T2DM subjects, while [PDE] is increased. Of note, these differences could not be appreciated using the traditional ratio method for *in vivo* ^{31}P-MRS. The strong correlation between [PCr] versus HbA1c, FPG and measures of insulin sensitivity and beta cell function supports

500 the concept that lower baseline skeletal muscle [PCr] is related to key determinants of
501 glucose homeostasis. Adoption of precise, quantitative ^{31}P-MRS measurements in
502 metabolic studies will allow this information to substantively contribute to modelling of
503 complex, *in vivo* metabolic processes in skeletal muscle (12).

Revised 02/27/2018

GRANTS

This work was supported by NIH grants DK24092-34 (RAD) and K25DK089012 (GDC).

REFERENCES

1. **Abdul-Ghani MA, Jenkinson CP, Richardson DK, Tripathy D, DeFronzo RA.** Insulin secretion and action in subjects with impaired fasting glucose and impaired glucose tolerance: Results from the veterans administration genetic epidemiology study. *Diabetes*. 55:1430-1435, 2006.

2. **Abdul-Ghani MA, DeFronzo RA**. Mitochondrial dysfunction, insulin resistance, and type 2 diabetes mellitus. *Curr Diab Rep*. 8:173-178, 2008.

3. **Abdul-Ghani MA, Muller FL, Liu Y, Chavez AO, Balas B, Zuo P, Chang Z, Tripathy D, Jani R, Molina-Carrion M, Monroy A, Folli F, Van Remmen H, DeFronzo RA.** Deleterious action of FA metabolites on ATP synthesis: Possible link between lipotoxicity, mitochondrial dysfunction, and insulin resistance. *Am J Physiol Endocrinol Metab*. 295: E678-85, 2008.

4. **Abdul-Ghani M, DeFronzo RA**. Is it time to change the type 2 diabetes treatment paradigm? Yes! GLP-1 RAs should replace metformin in the type 2 diabetes algorithm. *Diabetes Care*. 40:1121-1127, 2017.

5. **Arnold D, Matthews P, Radda G.** Metabolic recovery after exercise and the assessment of mitochondrial function in vivo in human skeletal muscle by means of ^{31}P NMR. *Magn Reson Med*. 1:307-315, 1984.

6. **Bajaj M, Suraamornkul S, Romanelli A, Cline GW, Mandarino LJ, Shulman GI, DeFronzo RA**. Effect of sustained reduction in plasma free fatty acid concentration on intramuscular long chain-fatty acyl-CoAs and insulin action in patients with type 2 diabetic patients. *Diabetes*. 54:3148-3153, 2005.

5327. **Bajaj M, Baig R, Suraamornkul S, Hardies LJ, Coletta D, Cline GW, Monroy A,**
533 **Musi N, Shulman GI, DeFronzo RA**. Effect of pioglitazone on intramocellular fat
534 metabolism in patients with type 2 diabetes mellitus. *J Clin Endo Metab.* 95:1916-1923,
535 2010.
5368. **Bays H, Mandarino L, DeFronzo RA**. Role of the adipocytes, FFA, and ectopic fat in
537 the pathogenesis of type 2 diabetes mellitus: PPAR agonists provide a rational
538 therapeutic approach. *J Clin Endocrinol Metab* 89:463-478, 2004.
5399. **Befroy DE, Petersen KF, Dufour S, Mason GF, de Graaf RA, Rothman DL,**
540 **Shulman GI.** Impaired mitochondrial substrate oxidation in muscle of insulin-resistant
541 offspring of type 2 diabetic patients. *Diabetes*. 56:1376-1381, 2007.
54210. **Belfort R, Mandarino L, Kashyap S, Wirfel K, Pratipanawatr T, Berria R, Cusi K,**
543 **DeFronzo RA**. Dose response effect of elevated plasma FFA on insulin signaling.
544 *Diabetes.* 54:1640-1648, 2005.
54511. **Boesch C, Machann J, Vermathen P, Schick F.** Role of proton MR for the study of
546 muscle lipid metabolism. *NMR Biomed*. 19:968-988, 2006.
54712. **Bordbar A, Monk JM, King ZA, Palsson BO**. Constraint-based models predict
548 metabolic and associated cellular functions. *Nat Rev Genetics*. 15:107-120, 2014.
54913. **Camporez JP, Wang Y, Faarkrog K, Chukijrungroat N, Petersen KF, Shulman GI**.
550 Mechanism by which arylamine N-acetyltransferase 1 ablation causes insulin resistance
551 in mice. *PNAS USA*. 114: E11285, 2017.
55214. **Daniele G, Eldor R, Merovci A, Clarke GD, Xiong J, Tripathy D, Taranova A, Abdul-**
553 **Ghani M, DeFronzo RA.** Chronic reduction of plasma free fatty acid improves

554 mitochondrial function and whole-body insulin sensitivity in obese and type 2 diabetic
555 individuals. *Diabetes*. 63:2812-20, 2014.
55615. **De Feyter HM, van den Broek, N M, Praet SF, Nicolay K, van Loon LJ, Prompers**
557 **JJ.** Early or advanced stage type 2 diabetes is not accompanied by in vivo skeletal
558 muscle mitochondrial dysfunction. *Eur J Endocrinol*. 158:643-653, 2008.
55916. **De Feyter HM, Lenaers E, Houten SM, Schrauwen P, Hesselink MK, Wanders RJ,**
560 **Nicolay K, Prompers JJ.** Increased intramyocellular lipid content but normal skeletal
561 muscle mitochondrial oxidative capacity throughout the pathogenesis of type 2 diabetes.
562 *FASEB J*. 22:3947-3955, 2008.
56317. **DeFronzo RA, Tobin JD, Andres R.** Glucose clamp technique: A method for
564 quantifying insulin secretion and resistance. *Am J Physiol*. 237: E214-23, 1979.
56518. **DeFronzo RA**. From the triumvirate to the ominous octet: a new paradigm for the
566 treatment of type 2 diabetes mellitus. *Diabetes*. 58:773-795, 2009.
56719. **Deiuliis JA**. MicroRNAs as regulators of metabolic disease: pathophysiologic
568 significance and emerging role as biomarkers and therapeutics. *Intl J Obesity*. 40:88-
569 101, 2016
57020. **Denton RM, Yorke RE, Randle PJ**. Measurement of concentrations of metabolites in
571 adipose tissue and effects of insulin, alloxan-diabetes and adrenaline. *Biochem J*.
572 100:407, 1966.
57321. **Dube JJ, Amati F, Stefanovic-Racic M, Toledo FG, Sauers SE, Goodpaster BH.**
574 Exercise-induced alterations in intramyocellular lipids and insulin resistance: The
575 athlete's paradox revisited. *Am J Physiol Endocrinol Metab*. 294: E882-8, 2008.

57622. **Foretz M, Hébrard S, Leclerc J, Zarrinpashneh E, Soty M, Mithieux G, Sakamoto K,**
577 **Andreelli F, Viollet B**. Metformin inhibits hepatic gluconeogenesis in mice
578 independently of the LKB1/AMPK pathway via a decrease in hepatic energy state. *J*
579 *Clin Invest.* 120, 2355–2369, 2010.
58023. **Goodpaster BH, He J, Watkins S, Kelley DE.** Skeletal muscle lipid content and insulin
581 resistance: Evidence for a paradox in endurance-trained athletes. *J Clin Endocrinol*
582 *Metab*. 86:5755-5761, 2001.
58324. **Harris R, Hultman E, Nordesjö L.** Glycogen, glycolytic intermediates and high-energy
584 phosphates determined in biopsy samples of musculus quadriceps femoris of man at
585 rest. methods and variance of values. *Scand J Clin Lab Invest*. 33:109-120, 1974.
58625. **Jensen JB, Gormsen LC, Sundelin E**. Organ-specific uptake and elimination of
587 metformin can be determined in vivo in mice and humans by PET-imaging using a novel
588 ^{11}C-metformin tracer. *Diabetes*. 64:128-LB (Suppl. 1), 2015.
58926. **Kelley DE, He J, Menshikova EV, Ritov VB**. Dysfunction of mitochondria in human
590 skeletal muscle in type 2 diabetes. *Diabetes*. 51:2944-50, 2002.
59127. **Kemp GJ, Thompson CH, Taylor DJ, Hands LJ, Rajagopalan B, Radda G**K.
592 Quantitative analysis by ^{31}P MRS of abnormal mitochondrial oxidation in skeletal muscle
593 during recovery from exercise. *NMR in Biomed*. 6: 302–310, 1993.
59428. **Kemp GJ, Meyerspeer M, Moser E.** Absolute quantification of phosphorus metabolite
595 concentrations in human muscle in vivo by 31P MRS: A quantitative review. *NMR*
596 *Biomed*. 20:555-565, 2007.

59729. **Knowles JW, Xie W, Zhang Z, Chennemsetty I, Assimes TL, Paananen J, Hansson**
598 **O, Pankow J, Goodarzi MO, Carcamo-Orive I, Morris AP**. Identification and validation
599 of N-acetyltransferase 2 as an insulin sensitivity gene. *J Clin Invest*. 125:1739-51, 2015.
60030. **Krssak M, Falk Petersen K, Dresner A, DiPietro L, Vogel SM, Rothman DL, Roden**
601 **M, Shulman GI.** Intramyocellular lipid concentrations are correlated with insulin
602 sensitivity in humans: a 1H NMR spectroscopy study. *Diabetologia*. 42:113-116, 1999.
60331. **Kurtz CL, Peck BC, Fannin EE, Beysen C, Miao J, Landstreet SR, Ding S, Turaga**
604 **V, Lund PK, Turner S, Biddinger SB**. MicroRNA-29 fine-tunes the expression of key
605 FOXA2-activated lipid metabolism genes and is dysregulated in animal models of
606 insulin resistance and diabetes. *Diabetes*. 63:3141-8., 2014.
60732. **Levin K, Schroeder HD, Alford FP, Beck-Nielsen H**. Morphometric documentation of
608 abnormal intramyocellular fat storage and reduced glycogen in obese patients with Type
609 II diabetes. *Diabetologia*. 44:824-33, 2001.
61033. **Matsuda M, DeFronzo RA.** Insulin sensitivity indices obtained from oral glucose
611 tolerance testing: Comparison with the euglycemic insulin clamp. *Diabetes Care*.
612 22:1462-1470, 1999.
61334. **Mogensen M, Sahlin K, Fernstrom M, Glintborg D, Vind BF, Beck-Nielsen H,**
614 **Hojlund K.** Mitochondrial respiration is decreased in skeletal muscle of patients with
615 type 2 diabetes. *Diabetes*. 56:1592-1599, 2007.
61635. **Morino K, Petersen KF, Dufour S, Befroy D, Frattini J, Shatzkes N, Neschen S,**
617 **White MF, Bilz S, Sono S, Pypaert M**. Reduced mitochondrial density and increased
618 IRS-1 serine phosphorylation in muscle of insulin-resistant offspring of type 2 diabetic
619 parents. *J Clin Invest*. 115:3587, 2005.

62036. **Musi N, Hirshman MF, Nygren J, Svanfeldt M, Bavenholm P, Rooyackers O, Zhou**
621 **G, Williamson JM, Ljunqvist O, Efendic S, Moller DE**. Metformin increases AMP-
622 activated protein kinase activity in skeletal muscle of subjects with type 2 diabetes.
623 *Diabetes*. 51:2074–2081, 2002.
62437. **Naressi A, Couturier C, Devos JM, Janssen M, Mangeat C, de Beer R, Graveron-**
625 **Demilly D.** Java-based graphical user interface for the MRUI quantitation package.
626 *MAGMA*. 12:141-152, 2001.
62738. **Newcomer BR, Larson-Meyer DE, Hunter GR, Weinsier RL**. Skeletal muscle
628 metabolism in overweight and post-overweight women: an isometric exercise study
629 using 31P magnetic resonance spectroscopy. *Intl J Obes*. 25:1309-1315, 2001.
63039. **Nowotny B, Zahiragic L, Krog D, Nowotny PJ, Herder C, Carstensen M, Yoshimura**
631 **T, Szendroedi J, Phielix E, Schadewaldt P, Schloot NC, Shulman GI, Roden M.**
632 Mechanisms underlying the onset of oral lipid-induced skeletal muscle insulin resistance
633 in humans. *Diabetes* 62:2240-2248, 2013.
63440. **Patti ME, Butte AJ, Crunkhorn S, Cusi K, Berria R, Kashyap S, Miyazaki Y, Kohane**
635 **I, Costello M, Saccone R, Landaker EJ, Goldfine AB, Mun E, DeFronzo R,**
636 **Finlayson J, Kahn CR, Mandarino LJ.** Coordinated reduction of genes of oxidative
637 metabolism in humans with insulin resistance and diabetes: Potential role of PGC1 and
638 NRF1. *Proc Natl Acad Sci U S A*. 100:8466-8471, 2003.
63941. **Petersen KF, Befroy D, Dufour S, Dziura J, Ariyan C, Rothman DL, DiPietro L,**
640 **Cline GW, Shulman GI.** Mitochondrial dysfunction in the elderly: Possible role in insulin
641 resistance. *Science*. 300:1140-1142, 2003.

642 42. **Petersen KF, Dufour S, Befroy D, Garcia R, Shulman GI.** Impaired mitochondrial
643 activity in the insulin-resistant offspring of patients with type 2 diabetes. *N Engl J Med*.
644 350:664-671, 2004.
645 43. **Praet SF, De Feyter HM, Jonkers RA, Nicolay K, van Pul C, Kuipers H, van Loon**
646 **LJ, Prompers JJ.** 31P MR spectroscopy and in vitro markers of oxidative capacity in
647 type 2 diabetes patients. *MAGMA*. 19:321-331, 2006.
648 44. **Regensteiner JG, Sippel J, McFarling ET, Wolfel EE, Hiatt WR.** Effects of non-insulin
649 dependent diabetes on maximal exercise performance. *Med Sci Sports Exerc.* 27: 875-
650 881, 1995.
651 45. **Ritov VB, Menshikova EV, He J, Ferrell RE, Goodpaster BH, Kelley DE**. Deficiency
652 of subsarcolemmal mitochondria in obesity and type 2 diabetes. *Diabetes.* 54:8-14,
653 2005.
654 46. **Ritov VB, Menshikova EV, Azuma K, Wood R, Toledo FG, Goodpaster BH,**
655 **Ruderman NB, Kelley DE.** Deficiency of electron transport chain in human skeletal
656 muscle mitochondria in type 2 diabetes mellitus and obesity. *Am J Physiol Endocrinol*
657 *Metab*. 298: E49-58, 2010.
658 47. **Roth K, Hubesch B, Meyerhoff D, Naruse S, Gober J, Lawry T, Boska MD, Matson**
659 **G, Weiner M.** Noninvasive quantitation of phosphorus metabolites in human tissue by
660 NMR spectroscopy. *J Magn Reson*. 81:299-311, 1989.
661 48. **Rothman DL, Shulman RG, Shulman GI**. ^{31}P nuclear magnetic resonance
662 measurements of muscle glucose-6-phosphate. Evidence for reduced insulin-dependent
663 muscle glucose transport or phosphorylation activity in non-insulin-dependent diabetes
664 mellitus. *J Clin Invest*. 89:1069-75, 1992.

549. **Schmid AI, Schrauwen-Hinderling VB, Andreas M, Wolzt M, Moser E, Roden M**. Comparison of measuring energy metabolism by different (31)P-magnetic resonance spectroscopy techniques in resting, ischemic, and exercising muscle. *Magn Reson Med.* 67: 898-905, 2012.

550. **Scheuermann-Freestone M, Madsen PL, Manners D, Blamire AM, Buckingham RE, Styles P, Radda GK, Neubauer S, Clarke K.** Abnormal cardiac and skeletal muscle energy metabolism in patients with type 2 diabetes. *Circulation*. 107:3040-3046, 2003.

551. **Schrauwen-Hinderling VB, Hesselink MK, Schrauwen P, Kooi ME.** Intramyocellular lipid content in human skeletal muscle. *Obesity (Silver Spring)*. 14:357-367, 2006.

552. **Schrauwen-Hinderling VB, Kooi ME, Hesselink MK, Jeneson JA, Backes WH, van Echteld CJ, van Engelshoven JM, Mensink M, Schrauwen P.** Impaired in vivo mitochondrial function but similar intramyocellular lipid content in patients with type 2 diabetes mellitus and BMI-matched control subjects. *Diabetologia*. 50:113-120, 2007.

553. **Schrauwen-Hinderling VB, Roden M, Kooi ME, Hesselink MK, Schrauwen P.** Muscular mitochondrial dysfunction and type 2 diabetes mellitus. *Curr Opin Clin Nutr Metab Care.* 10:698-703, 2007.

554. **Shaw CS, Jones DA, Wagenmakers AJ**. Network distribution of mitochondria and lipid droplets in human muscle fibres. *Histochem Cell Biol*. 129:65-72, 2008.

555. **Shulman GI**. Cellular mechanisms of insulin resistance. *J Clin Invest*. 106:171-176, 2000.

556. **Szendroedi J, Schmid AI, Chmelik M, Krssak M, Nowotny P, Prikoszovich T, Kautzky-Willer A, Wolzt M, Waldhäusl W, Roden M**. Skeletal muscle phosphodiester content relates to body mass and glycemic control. *PloS one*.14:6: e21846, 2011.

68857. **Szendroedi J, Yoshimura T, Phielix E, Koliaki C, Marcucci M, Zhang D, Jelenik T,**
689 **Muller J, Herder C, Nowotny P, Shulman GI, Roden M.** Role of diacylglycerol
690 activation of PKCtheta in lipid-induced muscle insulin resistance in humans. *Proc Natl*
691 *Acad Sci USA.* 111:9597-9602, 2014.
69258. **Team R**. R: A language and environment for statistical computing. 2013
69359. **van Loon LJ, Koopman R, Manders R, van der Weegen W, van Kranenburg GP,**
694 **Keizer HA.** Intramyocellular lipid content in type 2 diabetes patients compared with
695 overweight sedentary men and highly trained endurance athletes. *Am J Physiol*
696 *Endocrinol Metab*. 287: E558-65, 2004.
69760. **Valaparla SK, Gao F, Daniele G, Abdul-Ghani M, Clarke GD.** Fiber orientation
698 measurements by diffusion tensor imaging improve hydrogen-1 magnetic resonance
699 spectroscopy of intramyocellular lipids in human leg muscles. *J Med Imag*. 2:026002,
700 2015. DOI: 10.1117/1.JMI.2.2.026002
70161. **Valkovič L, Chmelík M, Ukropcová B, Heckmann T, Bogner W, Frollo I, Tschan H,**
702 **Krebs M, Bachl N, Ukropec J, Trattnig S**. Skeletal muscle alkaline Pi pool is
703 decreased in overweight-to-obese sedentary subjects and relates to mitochondrial
704 capacity and phosphodiester content. *Sci Rep*.6, 2016. DOI: 10.1038/srep20087
70562. **Wang X, Salibi N, Fayad LM, Barker PB**. Proton magnetic resonance spectroscopy of
706 skeletal muscle: a comparison of two quantitation techniques. *J Magn Reson* 243: 81-
707 84, 2014.
70863. **Ward SR, Lieber RL**. Density and hydration of fresh and fixed human skeletal muscle.
709 *J Biomech.* 38: 2317-2320, 2005.

64. **Wu FY, Tu HJ, Qin B, Chen T, Xu HF, Qi J, Wang DH.** Value of dynamic (31)P magnetic resonance spectroscopy technique in in vivo assessment of the skeletal muscle mitochondrial function in type 2 diabetes. *Chin Med J (Engl)*. 125:281-286, 2012.

FIGURE LEGENDS

Figure 1. (A) Depiction of ^{31}P-MRS experimental set-up based on axial ^{1}H-MR image of right leg used to guide placement of MRS slab. Note subject is prone and coil is attached to table to ensure reproducibility of results. (B) Representative ^{31}P-MR spectra from two 54-year-old women. Top: subject with T2DM Bottom: NGT subject. PCr and ATP peaks are noticeably lower in the T2DM skeletal muscle.

Figure 2. Inverse relationship between [PCr] and hemoglobin A1c (A) and fasting plasma glucose (B). Positive correlation between [PCr] and [ATP] in subjects with NGT and T2DM (C). Weak negative correlation between [PCr] and [PDE] is shown in (D). Subjects with NGT are represented by squares and T2DM subjects by diamonds.

Figure 3. Relationship between [IMCL] and hemoglobin A1c (A), Matsuda Index of insulin sensitivity (B) and insulin sensitivity index (M/I) measured with the insulin clamp (C) in subjects with NGT and T2DM. [IMCL] was also strongly and positively correlated with [PDE] obtained with ^{31}P-MRS. (D) NGT Subjects are denoted by squares and T2DM subjects by diamonds.

Figure 4. Relationships between [PDE] and hemoglobin A1c (A), fasting plasma glucose (B), Matsuda Index of insulin sensitivity (C), and the insulin sensitivity index (M/I) in subjects with NGT (squares) and T2DM (diamonds).

Revised 02/27/2018

Figure 5. Significant correlations were observed between mitochondrial density and three phosphorus metabolites: (A) [PCr]: r = -0.67, p = 0.009, (B) [ATP]: r = -0.63, p = 0.02, (C) [Pi]: r = -0.61, p = 0.02. Similar correlations were found when each group was examined individually. There was no correlation of [PDE] with mitochondrial density. Subjects with NGT are represented by squares and T2DM subjects by triangles.

Figure 6. Representative transmission electron micrographs at 15,000x. Left: a NGT (62 y.o. Male) subject and Tight: a T2DM (59 y.o. Male) subject showing mitochondria in longitudinal VL muscle fibers. These images are probably of slow twitch fibers, which are characterized by thick Z lines and mitochondria paired along either side in at regular intervals (black arrows). The T2DM sample on the right exhibits large lipid droplets (L) and a less regular mitochondrial arrangement.

Figure 7. Correlation between [PCr] and [IMCL] in T2DM: r = 0.72, p = 0.04 (A) and NGT: r = -0.77, p = 0.02 (B).

Figure 8. ATP synthesis rate in NGT and T2DM subjects.

Revised 02/27/2018

Table1. Clinical characteristics of the participants.

	NGT	T2DM	P-Value
Number	14	11	--
Sex (Males/Females)	7/7	7/4	--
Age (years)	47.0 ± 12.8	55.1 ± 11.1	0.14
Diabetes duration (years)	NA	3.8±1.5	
Weight (kg)	83.1 ±13.8	88.6 ± 13.1	0.33
BMI (kg/m^2)	28.6 ± 3.9	30.8 ± 5.0	0.22
FPG (mg/dl)	93 ± 6	140 ± 23	<0.001
HbA1c (%)	5.5 ± 0.3	7.5 ± 0.7	<0.001
Total Cholesterol (mg/dl)	173±38	173±57	0.99
LDL Chol (mg/dl)	99±39	93±41	0.73
HDL Chol (mg/dl)	56±12	37±5	<0.001
Triglycerides (mg/dl)	93±63	221±135	0.006
Matsuda Index of Insulin Sensitivity	4.76 ± 2.75	1.80 ± 1.18	0.003
IS/IR Index	5.91±2.95	0.66±0.71	<0.001
TGD (mg/kg.min)*	8.37 ± 2.07	4.39 ± 2.17	<0.001
TGD/SSPI (mg/kg.min) ÷ (uU/mL)	4.03 ± 1.52	1.77 ± 0.68	<0.001
Mitochondrial Density + (mito/μm^2)	0.19 ± 0.04	0.19 ± 0.02	0.96

IS/IR = Insulin secretion/Insulin resistance (disposition) index
TGD = total body glucose disposal; SSPI = steady state plasma insulin concentration
*Subset of 12 NGT and 9 T2DM participated in the euglycemic insulin clamp
+8 NGT and 6 T2DM subjects had muscle biopsies

Revised 02/27/2018

770

Table 2. Phosphorus metabolites measured by ^{31}P-MRS and intramyocellular lipid concentration (IMCL) by ^{1}H-MRS.

771

Parameter	NGT	T2DM	P-Value
[Pi](mM)	2.80 ± 0.57	2.79 ± 0.41	0.93
[ATP](mM)	7.18 ± 0.6	6.37 ± 1.05	0.02
[PCr](mM)	28.6 ± 3.2	24.6 ± 2.4	0.002
$[PCr]_{conv}$(mM)*	32.5 ± 1.7	32.2 ± 4.1	0.82
[PDE](mM)	3.11±0.82	4.04±0.98	0.02
$[PDE]_{conv}$(mM)*	3.72±1.05	5.35±1.6	0.005
pH	7.00 ± 0.03	7.00 ± 0.05	0.99
[Cr](mM)	21.8 ± 5.6	19.7 ± 2.5	0.28
[ADP](μM)	33 ± 9	31 ± 6	0.45
$[ADP]_{conv}$ (μM)**	26 ± 8	35 ± 9	0.03
[IMCL](mmol/kg)***	6.87 ± 1.15	8.99 ± 1.46	0.004

772

*$[PCr]_{conv}$ and $[PDE]_{conv}$ use the ratio of the desired metabolite to the amplitude of ATP x [ATP], using the assumption that $[ATP]_{conv}$ = 8.2 mM.

**$[ADP]_{conv}$ assumes $[ATP]_{conv}$ = 8.2 mM and [PCr]+[Cr] = 42.5 mM

***Determined in a subset of 9 NGT and 8 T2DM subjects

773
774
775
776

Revised 02/27/2018

FIGURE 1

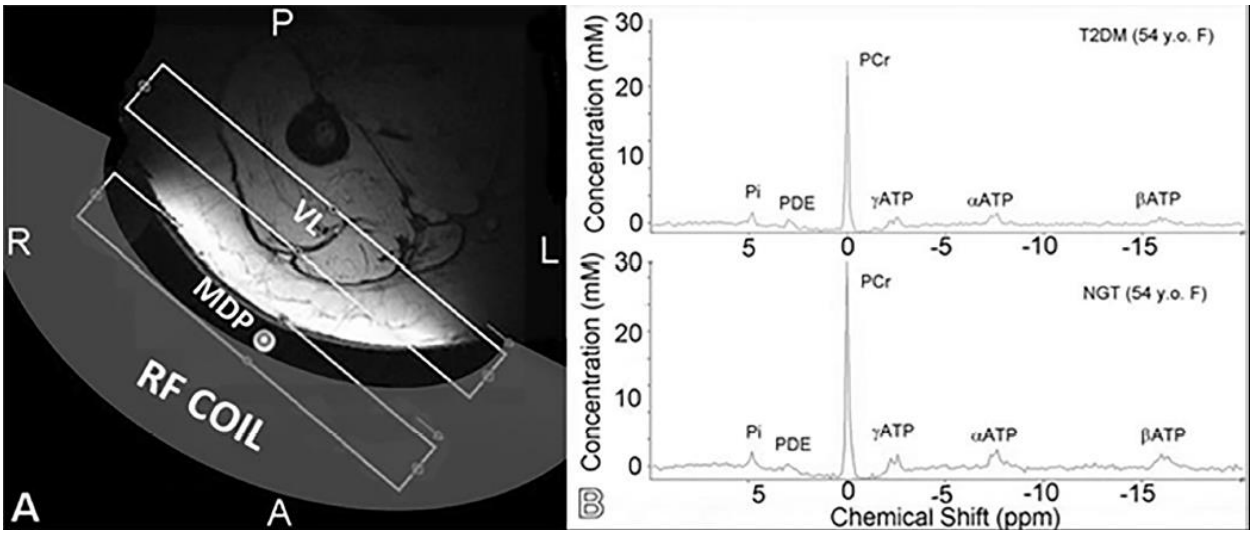

Figure 1. (A) Depiction of ^{31}P-MRS experimental set-up based on axial ^{1}H-MR image of right leg used to guide placement of MRS slab. Note subject is prone and coil is attached to table to ensure reproducibility of results. (B) Representative ^{31}P-MR spectra from two 54-year-old women. Top: subject with T2DM Bottom: NGT subject. PCr and ATP peaks are noticeably lower in the T2DM skeletal muscle.

Revised 02/27/2018

FIGURE 2

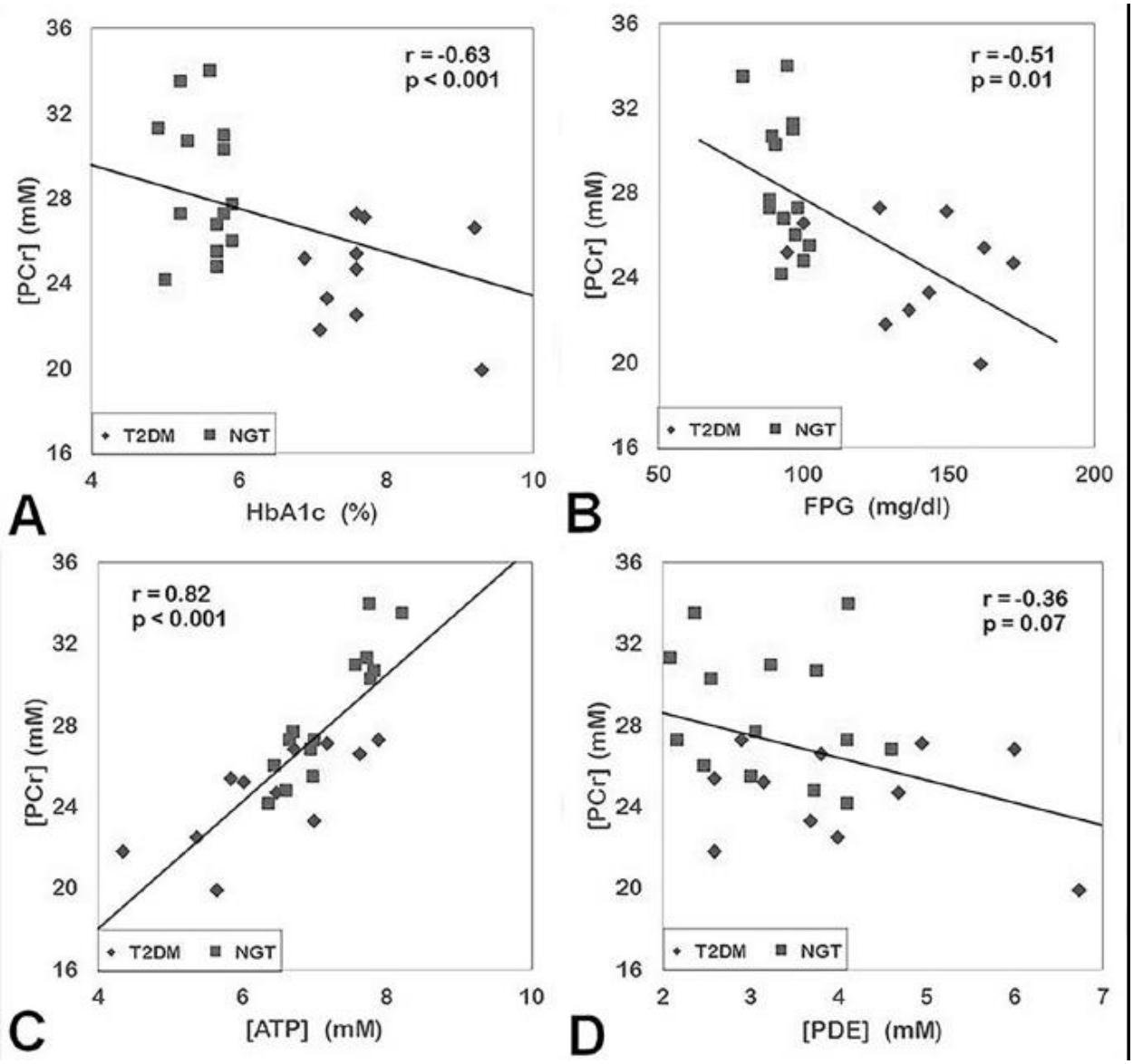

Figure 2. Inverse relationship between [PCr] and hemoglobin A1c (A) and fasting plasma glucose (B). Positive correlation between [PCr] and [ATP] in subjects with NGT and T2DM (C). Weak negative correlation between [PCr] and [PDE] is shown in (D). Subjects with NGT are represented by squares and T2DM subjects by diamonds.

Revised 02/27/2018

FIGURE 3

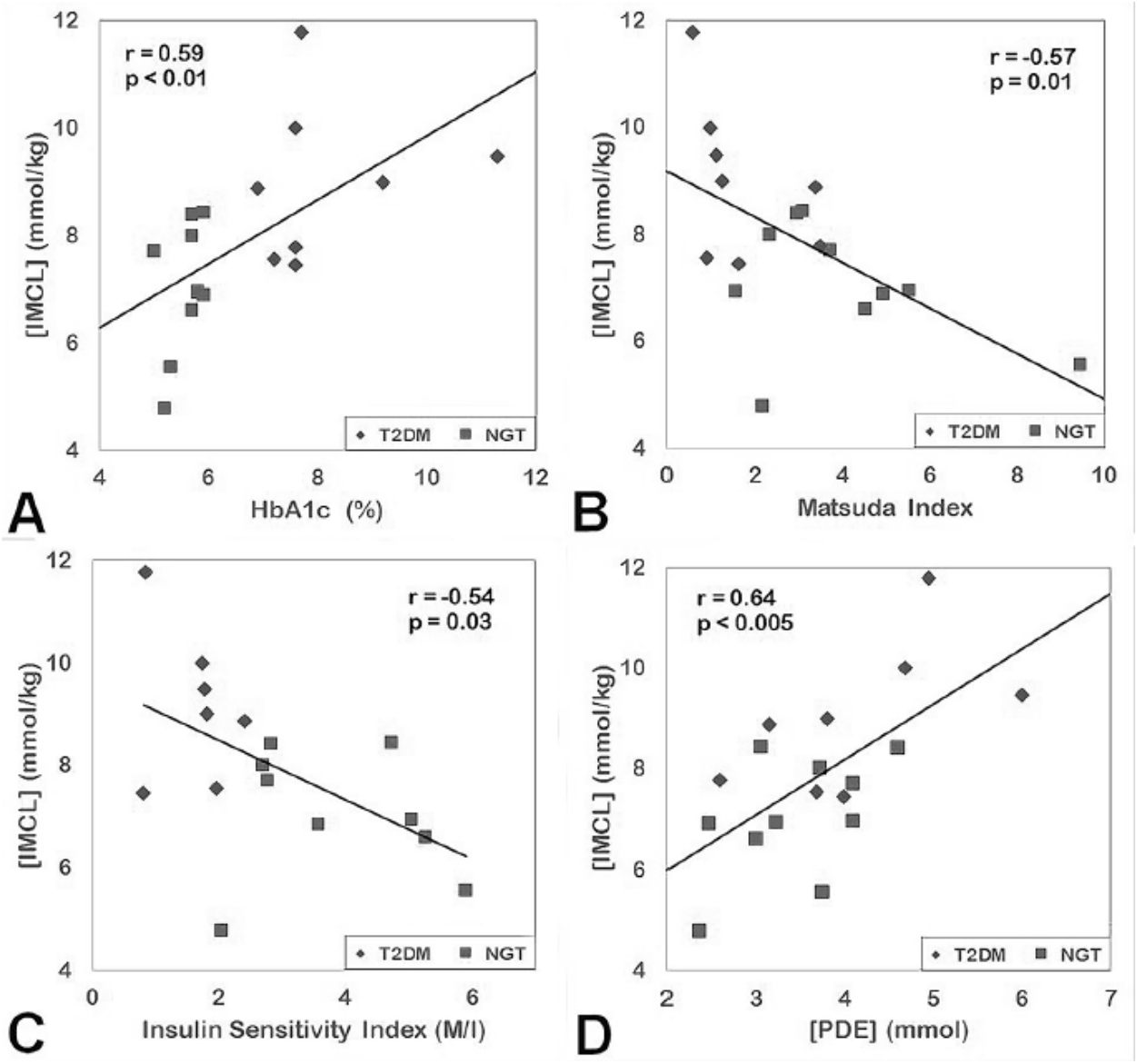

Figure 3. Relationship between [IMCL] and hemoglobin A1c (A), Matsuda Index of insulin sensitivity (B) and insulin sensitivity index (M/I) measured with the insulin clamp (C) in subjects with NGT and T2DM. [IMCL] was also strongly and positively correlated with [PDE] obtained with ^{31}P-MRS. (D) NGT Subjects are denoted by diamonds and T2DM subjects by circles.

FIGURE 4

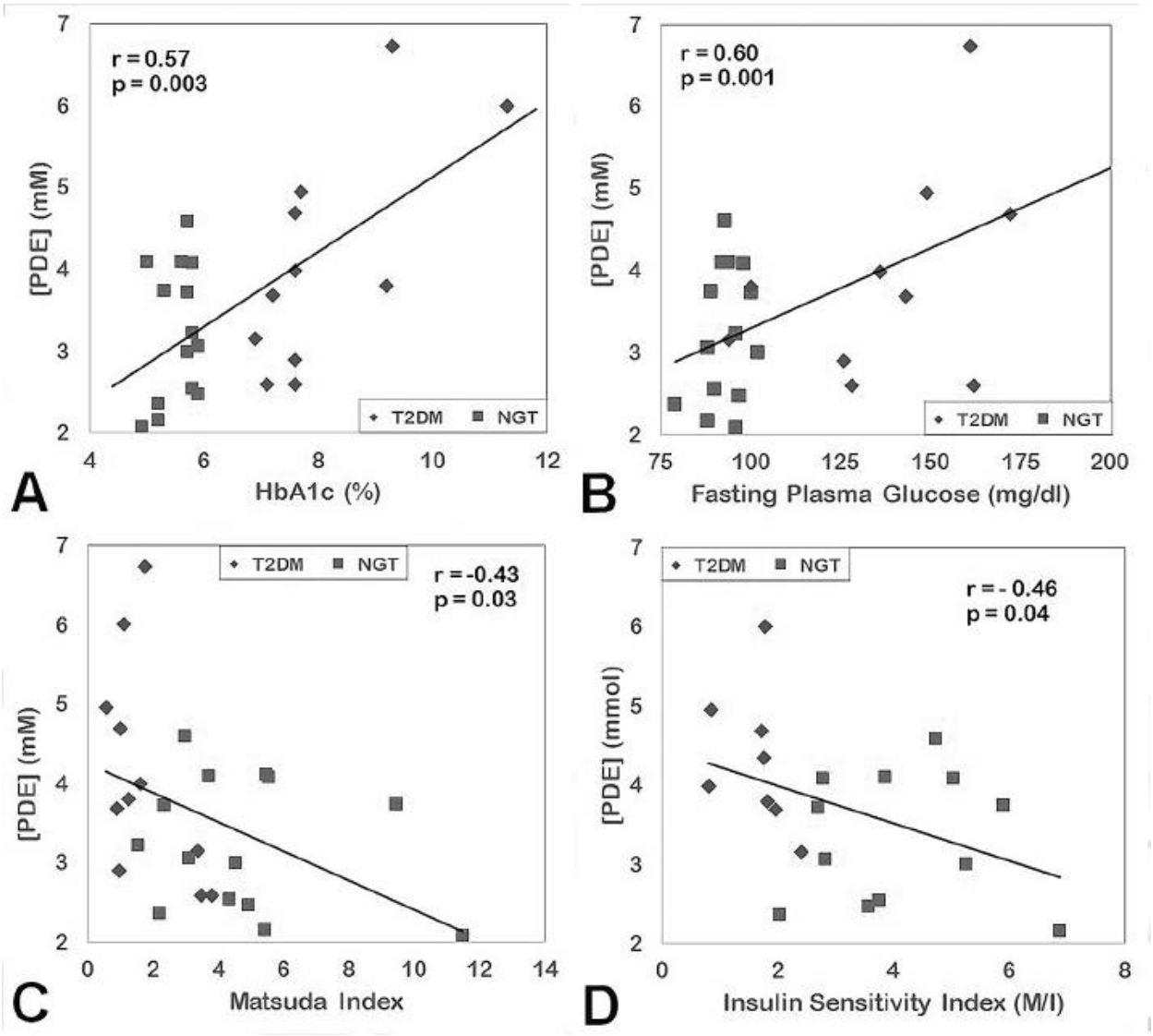

Figure 4. Relationships between [PDE] and hemoglobin A1c (A), fasting plasma glucose (B), Matsuda Index of insulin sensitivity (C), and the insulin sensitivity index (M/I) in subjects with NGT (squares) and T2DM (diamonds).

Revised 02/27/2018

FIGURE 5

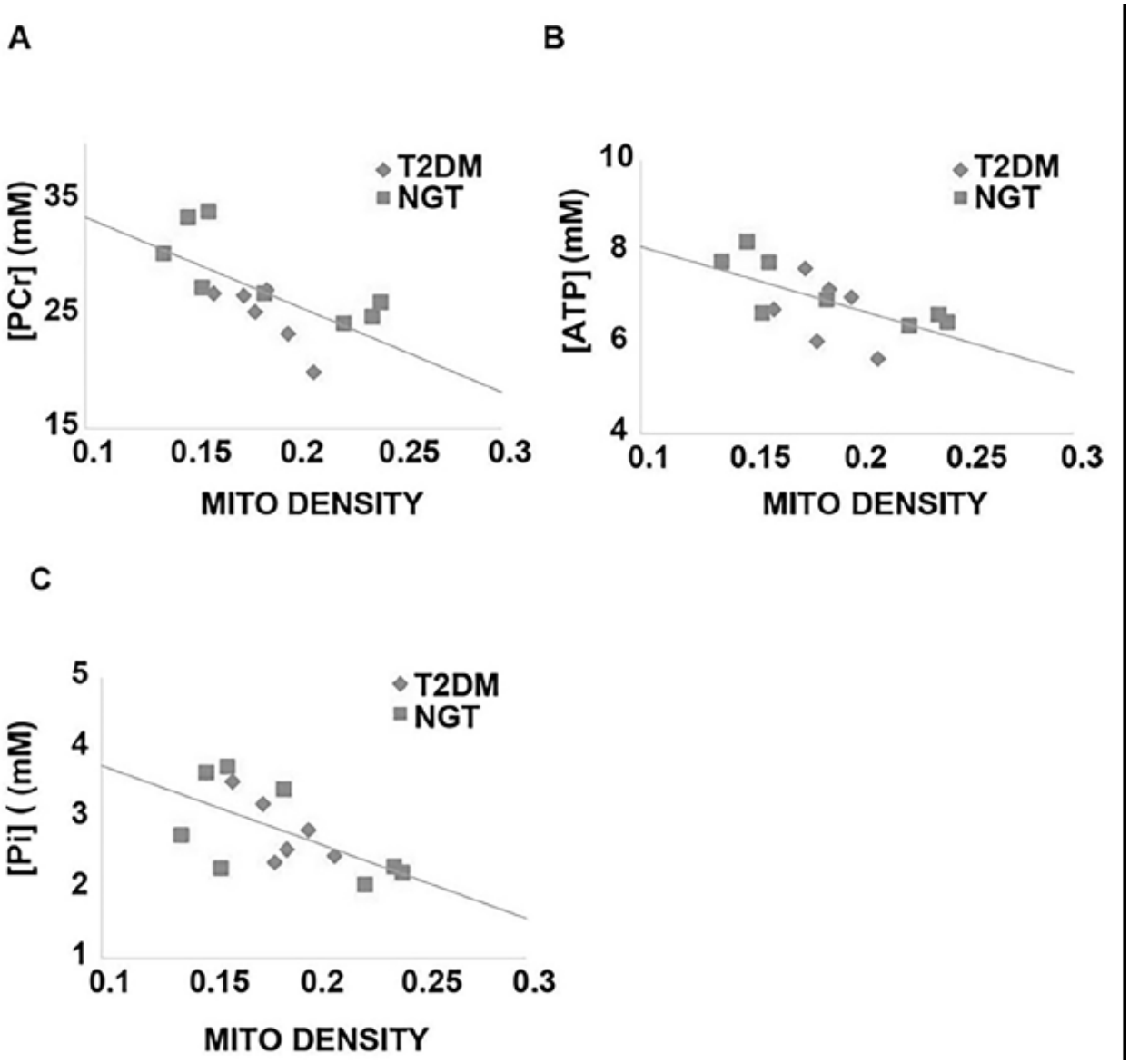

Figure 5. Significant correlations were observed between mitochondrial density and three phosphorus metabolites: (A) [PCr]: r = -0.67, p = 0.009, (B) [ATP]: r = -0.63, p = 0.02, (C) [Pi]: r = -0.61, p = 0.02. Similar correlations were found when each group was examined individually. There was no correlation of [PDE] with mitochondrial density. Subjects with NGT are represented by squares and T2DM subjects by diamonds.

Revised 02/27/2018

FIGURE 6

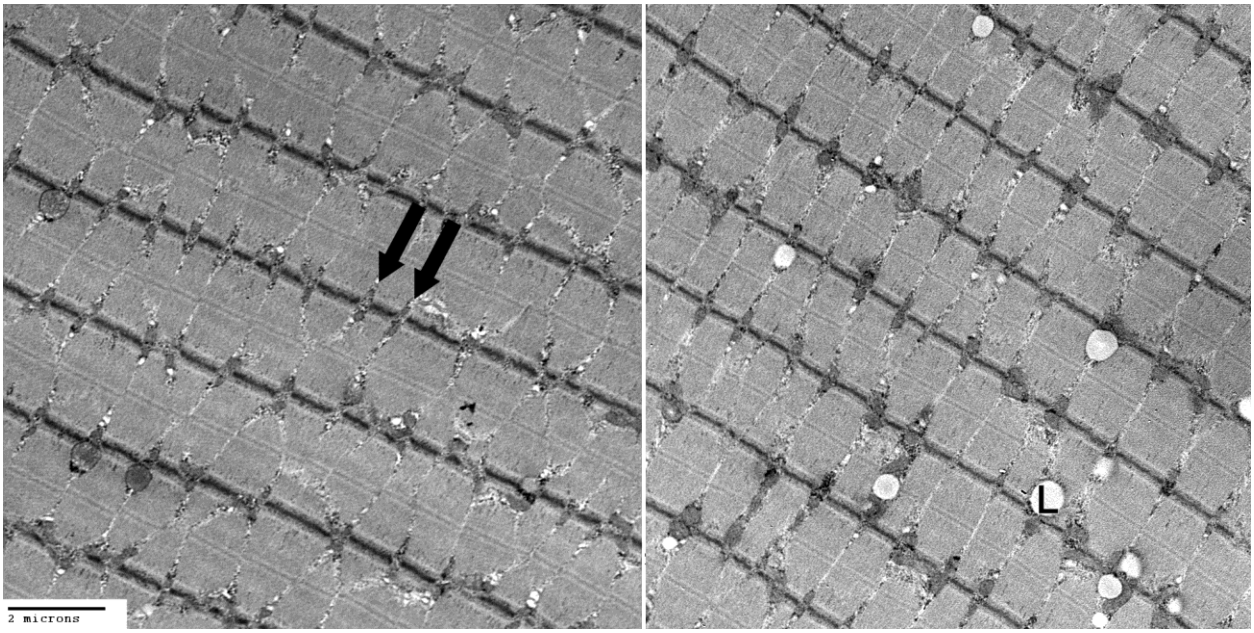

Figure 6. Representative transmission electron micrographs at 15,000x. Left: a NGT (62 y.o. Male) subject and Right: a T2DM (59 y.o. Male) subject showing mitochondria in longitudinal VL muscle fibers. These images are probably of slow twitch fibers, which are characterized by thick Z lines and mitochondria paired along either side in at regular intervals (black arrows). The T2DM sample on the right exhibits large lipid droplets (L) and slightly less regular mitochondrial arrangement.

Revised 02/27/2018

FIGURE 7

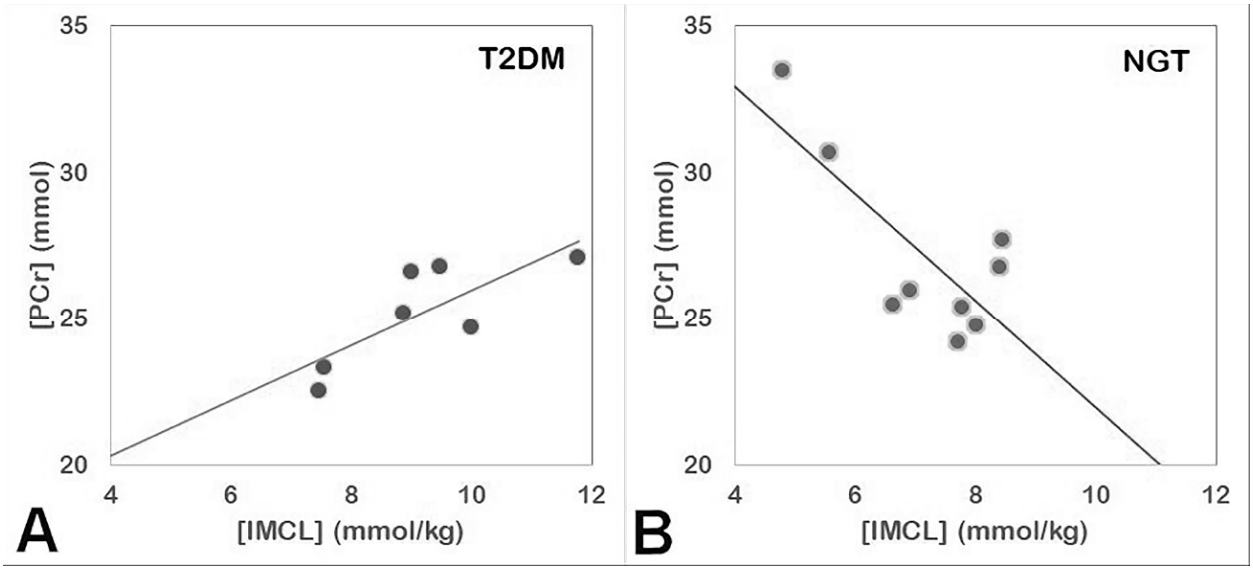

Figure 7. Correlation between [PCr] and [IMCL] in T2DM: r = 0.72, p = 0.04 (A) and NGT: r = -0.77, p = 0.02 (B)

Revised 02/27/2018

FIGURE 8

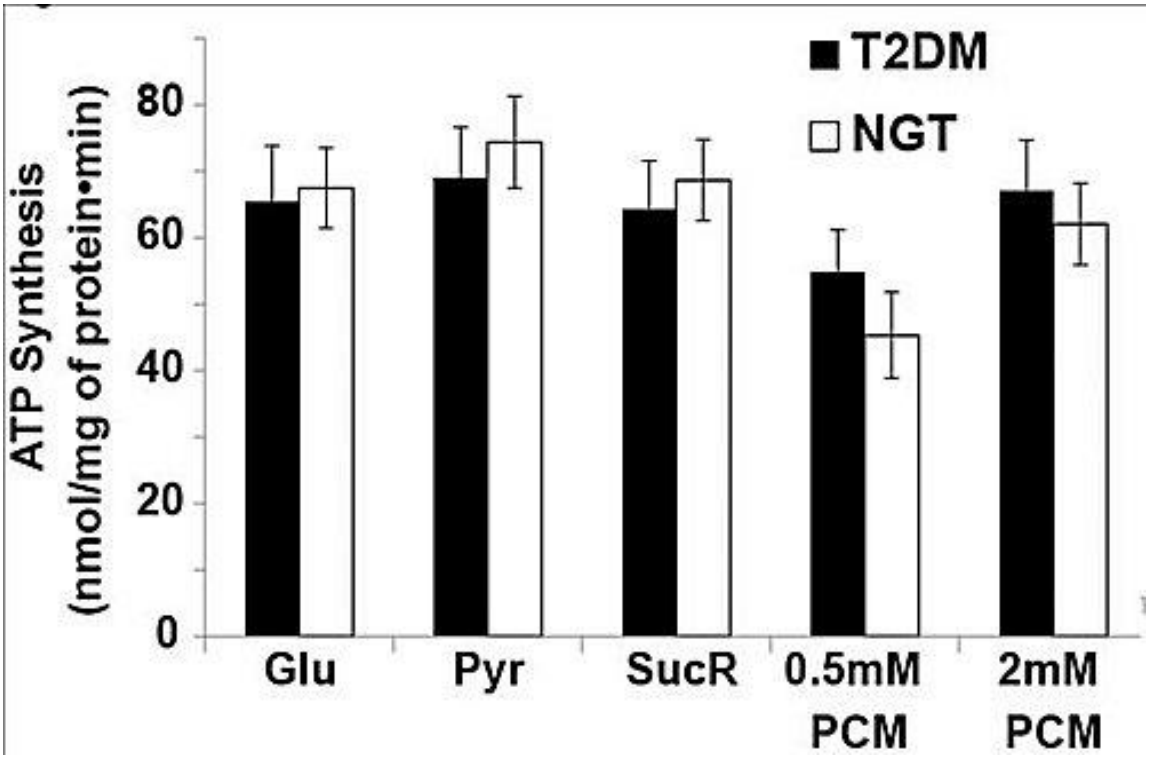

Figure 8. ATP synthesis rate in NGT and T2DM subjects

Revised 02/27/2018